Diffusional and vibrational dynamics of water in NaA zeolites by neutron and Fourier transform infrared spectroscopy

2004 J. Phys.: Condens. Matter 16 S5297

(http://iopscience.iop.org/0953-8984/16/45/001)

INSTITUTE OF PHYSICS PUBLISHING JOURNAL OF PHYSICS: CONDENSED MATTER

J. Phys.: Condens. Matter **16** (2004) S5297–S5316 PII: S0953-8984(04)74684-6

Diffusional and vibrational dynamics of water in NaA zeolites by neutron and Fourier transform infrared spectroscopy

V Crupi, D Majolino and V Venuti

Department of Physics, University of Messina, Contrada Papardo, Salita Sperone 31, PO Box 55, 98166 S Agata, Messina, Italy

E-mail: majolino@unime.it

Received 13 January 2004
Published 29 October 2004
Online at stacks.iop.org/JPhysCM/16/S5297
doi:10.1088/0953-8984/16/45/001

Abstract

This paper reports the most recent results of a detailed spectroscopic analysis of water confined in NaA zeolitic matrix, performed, as a function of temperature and hydration level, by means of the simultaneous use of incoherent quasi-elastic neutron scattering (IQENS) and Fourier transform infrared (FT-IR) absorption.

The diffusive process reveals a rather wide distribution of relaxation times. Furthermore, we observed a Q-dependence of the mean relaxation time $\langle\tau\rangle$ which does not disagree with the mode coupling theory for associated liquids. As far as vibrational dynamics is concerned, the spectral substructure of the H_2O bending (1500–1800 cm^{-1}) and O–H stretching (3000–3800 cm^{-1}) bands has been interpreted in the framework of actual theories for associated liquids and on the basis of previous measurements performed, by Raman scattering, on water confined in a controlled silica glass (GelSil). From a comparison of the results in these two cases, the 'structure-maker' role on confined water, played by the NaA zeolite, and the 'structure-breaker' role, played by the GelSil, have been clearly shown.

1. Introduction

Water, as the most important liquid, exhibits special properties owing to its ability to form a hydrogen-bond network with striking consequences for the biosphere, e.g., the anomalous melting and boiling points of this liquid. The physics of water is a subject with a long tradition in science [1].

Nevertheless, over recent years there has been a large theoretical and experimental interest devoted to the determination of the structure and dynamics of water adjacent to solid surfaces [2]. This can be explained by the fact that in many common situations water is attached

to some substrate or entrapped into small voids of porous media: water in a rock or sandstone, in the interior of a cell, in a microemulsion, at the surface of biological macromolecules and membranes constitute just a few examples. The knowledge of the dynamical behaviour of confined water, and its relation with the bulk state, is at the basis of the comprehension of many technological problems such as catalysis, tertiary oil recovery, corrosion inhibition, membrane separations, and other numerous electrochemical processes [3, 4]. In biology, in particular, it has been observed that the biological functionality of globular proteins or membranes is strongly dependent by the hydration level; in fact when the hydration level decreases, the functionality may be inhibited [5].

Recent literature reports on many studies performed on confined or interfacial water. Various model systems, with hydrophobic and hydrophilic inner surfaces, have been used to confine water, namely Vycor glasses [6–9], clay minerals [10], and porous silica glasses [11, 12]. In particular, in most of these studies, porous glasses, with pore dimensions ranging from 20 to 100 Å, have been used to obtain geometrically controlled confinements.

Several attempts have been reported to deduce structural and dynamical information on these systems by neutron [6–9, 11], light [12] and x-ray scattering [13], nuclear magnetic resonance (NMR) [14] and dielectric relaxation [15], as well as molecular dynamics (MD) simulations [16–18]. Experimental findings and theoretical approaches evidenced a slowed-down dynamics of confined water, justified in terms of the interplay between two competitive processes: surface interactions (chemical effect) and geometric restrictions (physical effect) [19]. Even if the scenario is not at the moment completely understood, because of the partial disagreement of the interpretation of the experimental findings coming from different techniques, it has been quite well established that confined water can easily be supercooled down to lower temperatures with respect to the bulk, and that the decrease of the hydration level gives rise to a diminishing of the nucleation temperature. Furthermore, MD simulations of supercooled water in Vycor glass, together with high resolution IQENS measurements of water at high temperatures confined in Vycor as well as in GelSil pores, showed that the low-frequency spectral region can be described in terms of the α-relaxation dynamics predicted by mode coupling theory (MCT) of supercooled liquids [9, 11, 20, 21].

In particular, some years ago, our research group performed a detailed analysis, as a function of temperature and hydration level, by means of light (Rayleigh wing, Raman) [12, 22] and neutron (incoherent quasi-elastic and inelastic neutron scattering, IQENS and IINS, respectively) [11, 22, 23] scattering, of dynamical properties of water in 26 Å diameter pores of a GelSil glass, a sol–gel controlled porous glassy matrix with a huge number of Si–OH groups on the inner surface, strong active sites for the H-bond with the water molecules. We showed that confinement strongly influences both the low-frequency quasi-elastic and inelastic contributions, and the fundamental intramolecular OH stretching mode. Our data revealed a distribution of relaxation times for reorientational motions, well described by a Havriliak–Negami profile, as a consequence of the formation of transient extended structures, because of the presence of the H-bond. Furthermore, as far as vibrational dynamics is concerned, we revealed the disappearance of the 60 and 170 cm^{-1} lattice bands in the effective Raman vibrational density of states (VDOS) in the restricted translational region, and the diminishing of the collective contribution to the polarized OH stretching band, connected to the fully bonded tetrahedral network, with the decreasing of the hydration percentage of water in the pores. IINS data for confined water evidenced, if compared to the bulk state, a flattening and attenuation of the hindered translational modes, at about 8 and 20 meV, and an enhancement of the librational mode at about 91 meV, confirming, in agreement with Raman measurements, that confinement seems to induce strongly destructive effects in interfacial water, where hydration

phenomena give rise to different environments evidenced by new spectral features, and loss of the tetrahedral environments (ice like), typical of pure liquid water.

All these results gave clear evidence of the 'structure-breaker' effect of this sol–gel matrix on H_2O molecules, as a consequence of the specific interaction (H-bond) between the encaged water and the silanol Si–OH active groups, that essentially destroys the intermolecular network of water.

In the last few years, many workers have been interested in studying the behaviour of water in zeolites [24, 25], crystalline materials with a network of uniform interconnected pores with a small pore diameter (∼10 Å). Zeolite investigators, in fact, have been concerned so far with many attractive applications of these synthetic systems, such as catalysts, molecular sieves, gas absorbents, ion exchangers, and fillers for many plastics and paper products. Furthermore, the zeolite–water couple provides a good combination for effective use of low temperature heat sources such as solar energy and waste heats from factories; that is, for energy saving [24]. Every zeolite is constituted by a three-dimensional rigid framework of alumino-silicate, with large voids having water molecules 'regularly' clustered with cations. Its general chemical formula can be written as $A_x^{\nu+}[Al_{\nu x}Si_yO_{2(\nu x+y)}]\cdot nH_2O$, in which A indicates cations with valence $\nu+$, of mainly alkaline or alkaline earth ions, sometimes a mixture of them, rarely transition metals. Since they can be easily exchanged with other kinds of cations in the solutions without changing the basic structure of the zeolite, the A ions are often called 'exchangeable ions'. Water molecules are also dehydrated without changing the framework structure until a temperature characteristic of the zeolite is reached. The heat exchange property is induced from the desorption/absorption of water molecules from/into the zeolites. Water occluded in the small voids formed in the alumino-silicate framework of zeolite is usually named 'zeolitic water', and its physicochemical nature is recognized to be in the middle between liquid and crystalline water. Its calculated entropy value results to be much lower than the one of liquid and ice, and for this reason some authors choose to define zeolitic water as a 'new state of water' [24].

We report here the most recent results on diffusional and vibrational properties of water confined in NaA zeolite, as obtained from IQENS and FT-IR absorption measurements, discussed as a function of temperature and hydration level. The high resolution IQENS data have been interpreted in the light of the confined diffusion model (CDM), based on the well-known random jump diffusion model for confined diffusion [26], and the relaxing cage model (RCM), that takes into account the α-relaxation dynamics predicted by mode coupling theory (MCT) of supercooled liquids [9, 27]. Furthermore, FT-IR absorption data in the H_2O bending and O–H stretching region have been analysed in the framework of actual theories based on the assignment of the various contributions to the different structural arrangements whose dynamics is driven by the H-bond [28]. The presence, for confined water, of sub-bands typical of the bulk state allowed us to hypothesize the 'structure-maker' role of the zeolite surface on physisorbed water. In particular, as far as the FT-IR spectra in the O–H stretching region are concerned, by a comparison with our already cited Raman measurements of water in GelSil, we unambiguously show the contrasting role played by the two confining matrices on the water vibrational dynamics.

2. Experimental details

We performed IQENS and FT-IR absorption measurements on water confined in ultrapure NaA zeolites (or Na-LTA as an abbreviation of the sodium form of the Linde Type A zeolite), purchased from Nippon Chemical Industrial Co., Ltd, in full ($27H_2O$ molecules) and partial ($6H_2O$ molecules) hydration conditions, as a function of temperature.

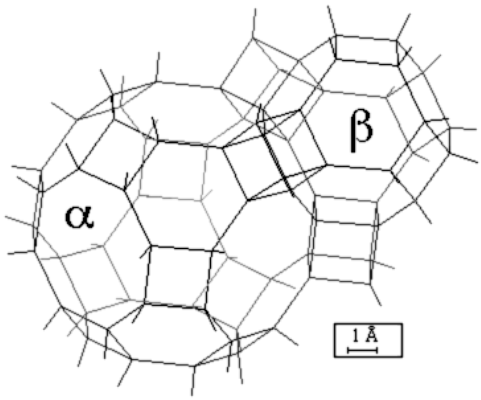

Figure 1. The skeletal framework of NaA-type zeolite. α- and β-cages are also shown.

The formula unit of NaA-type zeolite is $Na_{12}Al_{12}Si_{12}O_{48}{\cdot}27H_2O$, as recognized, some years ago, by Gramlich and Meier [29], by means of a very careful x-ray diffraction study. As a result, they singled out, in the framework, larger α-cages (representing a pentagonal dodecahedron of radius $r \sim 5$ Å) and smaller β-cages (cubooctahedral cage) in which the water molecules are located (see figure 1). They observed five sites available for water molecules in the zeolitic structure. Site I, inside the small β-cage, appears to be occupied by four water molecules, originating a distorted tetrahedron; sites II and III, inside the α-cage, are occupied by about 20 water molecules. The contents of site IV within the eight-membered ring windows provide the linkages between the water polyhedra. Another broad peak, revealed at the centre of the dodecahedral cluster, has been identified as site V, probably generated by a less symmetrical arrangement involving more than one atom, possibly one H_2O molecule and one Na ion.

IQENS data were collected, in full hydration conditions at $T = 253$, 273, 293, 313 K, at the ISIS pulsed neutron source at the Rutherford Appleton Laboratory (RAL), UK, by means of the high resolution IRIS spectrometer. The investigated Q-range was $0.96-3.698$ Å^{-1}, with a mean energy resolution $\Delta E = 27.2$ μeV (hwhm). The polycrystalline samples were contained between two thin aluminium sheets in the form of 40×40 mm^2 slabs with thickness small enough to avoid multiple scattering corrections. The data have been corrected for the empty cell with dehydrated zeolite, sample absorption, detector efficiency, and then transformed to an energy scale using standard programs available at ISIS. Taking into account the chemical structure of the samples, the total scattering will be dominated by the large incoherent scattering cross section of hydrogen. This means that we are looking at the self-diffusion of the protons, and measuring the incoherent structure factor $S_{\mathrm{inc}}(Q, \omega)$.

Infrared absorption spectra were collected, in full hydration conditions at $T = 278$, 293, 313, 333, 353 K and, as a comparison, in partial hydration conditions at $T = 293$ K, by a BOMEM DA8 Fourier transform infrared (FT-IR) spectrometer, working with a globar lamp source, a KBr beamsplitter, and a DTGS/KBr detector. The powdered samples were reduced in pellets in order to be analysed by mixing 2 mg of zeolite in 180 mg of caesium iodide, CsI, transparent in the range of interest. The H_2O bending (1500–1800 cm^{-1}) and O–H stretching (3000–3800 cm^{-1}) regions have been analysed, with a resolution of 4 cm^{-1}, automatically adding 32 repetitive scans in order to obtain a good signal to noise ratio and high reproducibility in the spectra. All the IR spectra were normalized for taking into account the effective number of adsorbers. By recalling the well-known Lambert–Beer absorbance law,

the absorbance (ABS) can be expressed in the following way:

$$\mathrm{ABS} = \log_{10}\left(\frac{\mathrm{REF}}{\mathrm{SPC}}\right) \tag{1}$$

where REF is the spectrum of the reference matrix (CsI pellets in our case) and ABS is the spectrum of the CsI matrix together with the sample itself (180 mg of CsI pellets + 2 mg of NaA zeolite $\times$ $27H_2O$, or 180 mg of CsI pellets + 2 mg of NaA zeolite $\times$ $6H_2O$).

3. Results and discussion

3.1. Diffusional dynamics: IQENS data

Our experimental IQENS spectra of both hydrated and dehydrated zeolites contain, in principle, a contribution from the zeolitic matrix and another due to the zeolitic water. However, the observed spectra of dehydrated NaA zeolites are constituted only by a narrow elastic line which can be represented by a δ-line (Dirac function) with a constant area A that is Q-independent, convolved with the instrumental resolution. This indicates a small contribution of the zeolitic framework to the total scattering. Its percentage was estimated, by calculating the cross sections of the zeolite constituents, to be 6% of the total scattered intensity. On these bases the spectra of dehydrated zeolites have been subtracted from the hydrated ones before proceeding with the best fit. As we said in the first section, the fitting procedure has been performed according to two different models: the confined diffusion model (CDM) and the relaxing cage model (RCM). The CDM model has been used in several publications in recent years for describing the translational diffusional dynamics in confined or interfacial water [8, 11, 30, 31]. It is based on the well-known Volino–Dianoux model, valid for the simple diffusion localised by a potential with spherical symmetry [26]. Nowadays, the RCM model is quite commonly recognized to be also appropriate to describe the diffusional dynamics in supercooled and interfacial water [32]. It essentially uses an idea borrowed from MCT. This latter is based on the cage effect present in the liquid state, which can be seen as a transient trapping of molecules by their neighbours. The cage can be a consequence of the distorted tetrahedral H-bond, formed by neighbouring environments, which tends to grow when T diminishes, originating a transient network whose lifetime is imposed by the finite H-bond lifetime ($\sim$1 ps at $T = 20\,^{\circ}\mathrm{C}$) [33].

The CDM model. In the framework of the CDM model, IQENS data have been fitted by the law

$$S_{\mathrm{S}}(Q,\omega) = A_{\mathrm{tot}}\left[A(Q)\delta(\omega) + (1 - A(Q))\,L(\omega)\right] \otimes \mathrm{Re}\,s + \mathrm{Bkg}. \tag{2}$$

As can be seen, the spectral line shape is the weighted superposition of an elastic peak, a δ-line, $\delta(\omega)$ with a Q-dependent fractional area $A(Q)$, and a quasi-elastic one, a Lorentzian profile, $L(\omega)$, having a fractional area given by $(1 - A(Q))$, reflecting translational and rotational motions, convoluted with the instrumental resolution. Bkg indicates a flat background. Just as an example we report, in figure 2, the typical high resolution IQENS data for NaA zeolite $\times$ $27H_2O$ at $T = 313$ K, as a function of Q, analysed by the CDM model.

Figure 3 reports, for the same sample, the behaviour, as a function of T, of the extracted half width at half maximum (hwhm), Γ, of the quasi-elastic Lorentzian contribution. The data are plotted as a function of Q^2. In analogy with the typical confined dynamics observed in nafion [34], vycor [8], proteins [35], and so on, there is, because of confinement, definite evidence of an initial plateau extending up to a Q^* value that gives a first idea of the inverse of the dimension d^* of the confining region. Then, the Γ values increase, revealing a diffusion inside the confining region, and tend to another constant value in the limit of very large Q.

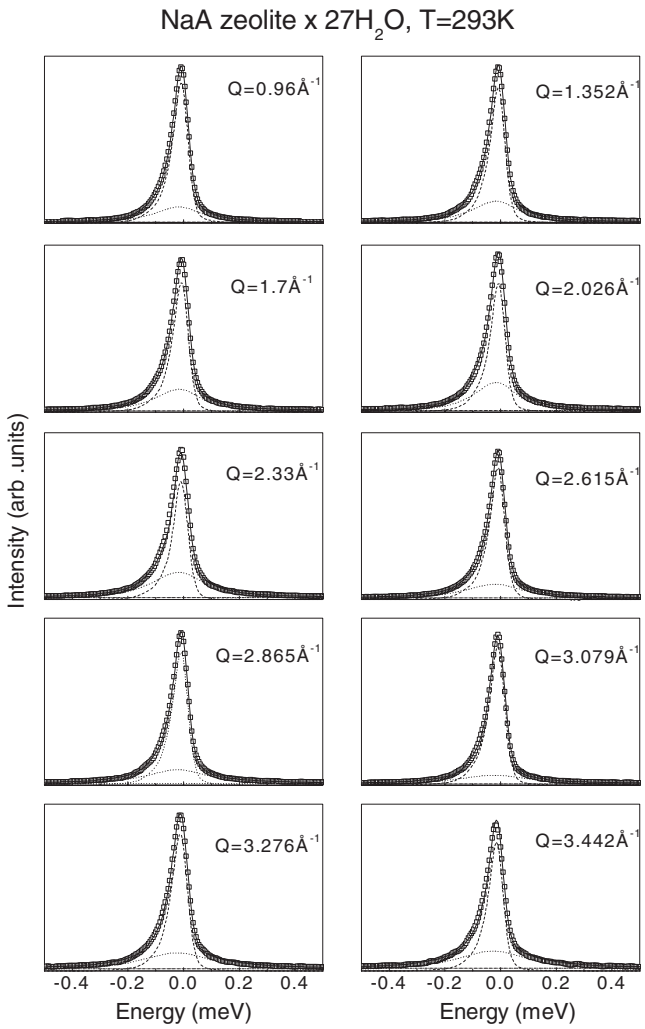

Figure 2. Experimental spectra (squares) from an IQENS experiment on NaA zeolite $\times$ $27H_2O$, at $T = 293$ K, for all the investigated Q-range, together with the best fit (solid curve) according to the CDM model and the deconvolution components (dashed curves).

For our system, the two features are clearly differentiated at $Q^* \sim 2.02$ Å^{-1}, a not surprising value considering the structure of the zeolite. This very high Q value from which the diffusive contribution to the IQENS spectra starts indicates that we are in presence of a *local* diffusion process, an occurrence that recalls the 'flip-flop' H-bond process of the proton tunnelling observed in ice.

The plateau at low Q has been, first of all, accounted for making reference to the Volino–Dianoux model for diffusion in a potential of spherical symmetry, hypothesizing approximately a diffusion of water in a sphere of radius a [26]. The dimension of the confining region has been obtained by $l^* = 2a = 2\pi Q^{*-1}$. We found, at all the investigated temperatures, $l^* = 3.11$ Å, a value comparable with the typical dimension of a water molecule. The model also predicts that the hwhm of $L(\omega)$ at $Q = 0$ is given by $4.33 D_{\text{local}}/a^2$, allowing us to estimate the diffusion coefficient within the confining volume, D_{local}. The extracted values are reported in table 1.

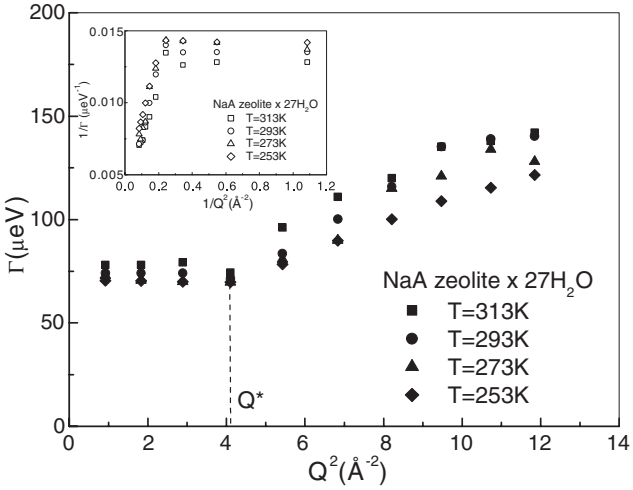

Figure 3. Linewidth (hwhm) Γ of the diffusive Lorentzian contribution of NaA zeolite $\times$ $27H_2O$ plotted, as a function of Q^2, for all the analysed temperatures. In the inset, the $1/\Gamma$ versus $1/Q^2$ plot is also reported.

Table 1. Relevant parameters for NaA zeolite $\times$ $27H_2O$ obtained in the framework of the CDM model. D_{local} is the diffusion constant in the localization volume; D is the diffusion coefficient for confined water; τ_0 is the residence time before jump for confined water, and finally D_{bulk} is the diffusion coefficient for bulk water as given by literature [1].

T (K)	D_{local} ($\times 10^{-5}$ cm^2 s^{-1})	D ($\times 10^{-5}$ cm^2 s^{-1})	τ_0 (ps)	D_{bulk} ($\times 10^{-5}$ cm^2 s^{-1})
253	0.54	0.39	3.4	0.43
273	0.56	0.41	3.2	1.10
293	0.57	0.43	3.1	2.03
313	0.60	0.48	3.0	3.20

Furthermore, taking into account that water molecules are forced to diffuse through interconnected pores, the same data have also been tentatively fitted in the framework of the Dianoux–Pineri–Volino model for confined diffusion inside a cylinder of radius a and height L [34]. Considering that the minimum dimension of the cylinder ($2a$ or L) cannot be smaller than the diameter of a sphere occupied by a rotating water molecule ($\sim$3 Å), we tried to fit our spectra for different axial ratios $\delta = L/2a$, and it turned out that the best fit was obtained for $2a \sim 3$ Å and $L \sim 3$ Å, restoring the spherical case.

On the basis of the above considerations we can hypothesize, for water molecules, a diffusion inside a spherical confining region of dimension $l^* = 3.11$ Å, definitively lower than the geometric confinement dimension (10 Å diameter pores). This occurrence can be explained by hypothesizing that immobile H_2O molecules are directly attached to the zeolite walls, as revealed also by x-ray diffraction [13], so causing a strong reduction to the available space for free diffusion.

In the inset of figure 3 we plot $1/\Gamma$ versus $1/Q^2$. From an inspection of the linear trend observed in the $Q > Q^*$ region, a random jump diffusion behaviour can be hypothesized. As is well known, it is given by

$$\Gamma(Q) = \frac{DQ^2}{1 + DQ^2\tau_0} \tag{3}$$

where τ_0 is the residence time before jump and D the diffusion coefficient. The values of τ_0 and D, reported in table 1, have been obtained, respectively, from the intercept and the slope of the linear variation of the curve $1/\Gamma$ as a function of $1/Q^2$. In particular (see table 1), the diffusion constants D are found to be smaller than the ones of bulk H_2O at the same temperature, and also smaller than the ones that we revealed studying the diffusion of water in 25 Å diameter pores of GelSil glass [11]. The estimated error in the best fit parameters determination is approximately 20% at low T, and 5% at higher and higher temperatures. We remark that, because of the wide Q-range covered for extracting D, its values appear to be more reliable than D_{local}, this latter also resulting from a model that considers impermeable walls (that is not exactly the case) and cavities bigger than the molecular dimension. As a confirmation of this we will see that the FT-IR data also give evidence of a tetrahedral structure, which is at the basis of the random jump diffusion model.

Concerning the residence times τ_0, an Arrhenius dependence, versus T, has not been revealed in the explored range.

The RCM model. A detailed discussion of the model has been given in [9] and will not be reported here. Briefly, we can say that the RCM model considers the central spectral feature of the incoherent neutron scattering from interfacial water as a single quasi-elastic peak arising from a distribution of relaxation times extending up to a timescale of picoseconds.

It has been shown that the intermediate scattering function can be written as

$$F_{\text{S}}(Q,t) = A(Q)\exp\left[-\left(\frac{t}{\tau}\right)^{\beta}\right]. \tag{4}$$

As can be seen, the relaxation is described by a non-exponential decay, characterized by a correlation time τ, related to the lifetime of the cage, and a stretched exponent β.

The dynamic structure factor of interfacial water is given by the expression

$$S_{\text{S}}(Q,\omega) = [\text{HN}(\omega)] \otimes \text{Re}\, s(\omega) + \text{Bkg}. \tag{5}$$

$\text{HN}(\omega)$ represents the Havriliak–Negami distribution function, characterized by τ_{HN} as the relaxation time, and α and γ (ranging between 0 and 1) as shape parameters [36, 37]:

$$\text{HN}(\omega) = -(1/\omega)\,\text{Im}\left[1 + (\text{i}\omega\tau_{\text{Hn}})^{\alpha}\right]^{-\gamma}. \tag{6}$$

The role it plays in the frequency domain is almost analogous to the one played by the Kolrausch–Williams–Watt $\text{KWW}(t)$ profile

$$\text{KWW}(t) = \exp\left[-\left(\frac{t}{\tau_{\text{KWW}}}\right)^{\beta}\right] \tag{7}$$

in the time domain. τ_{KWW} is a characteristic relaxation time and the stretched exponent β gives the width of the distribution.

The relevant parameters of $\text{HN}(\omega)$ and $\text{KWW}(t)$ are related by

$$\log(\tau_{\text{HN}}/\tau_{\text{KWW}}) = 2.6(1-\beta)^{0.5}\exp(-3\beta) \tag{8}$$

as far as the characteristic relaxation times are concerned, and

$$\alpha\gamma = \beta^{1.23} \tag{9}$$

for the shape parameters.

The mean relaxation time $\langle\tau\rangle$ of the distribution is defined as

$$\langle\tau\rangle = \left(\frac{\tau_{\text{KWW}}}{\beta}\right)\Gamma\left(\frac{1}{\beta}\right) \tag{10}$$

Γ being the Gamma function.

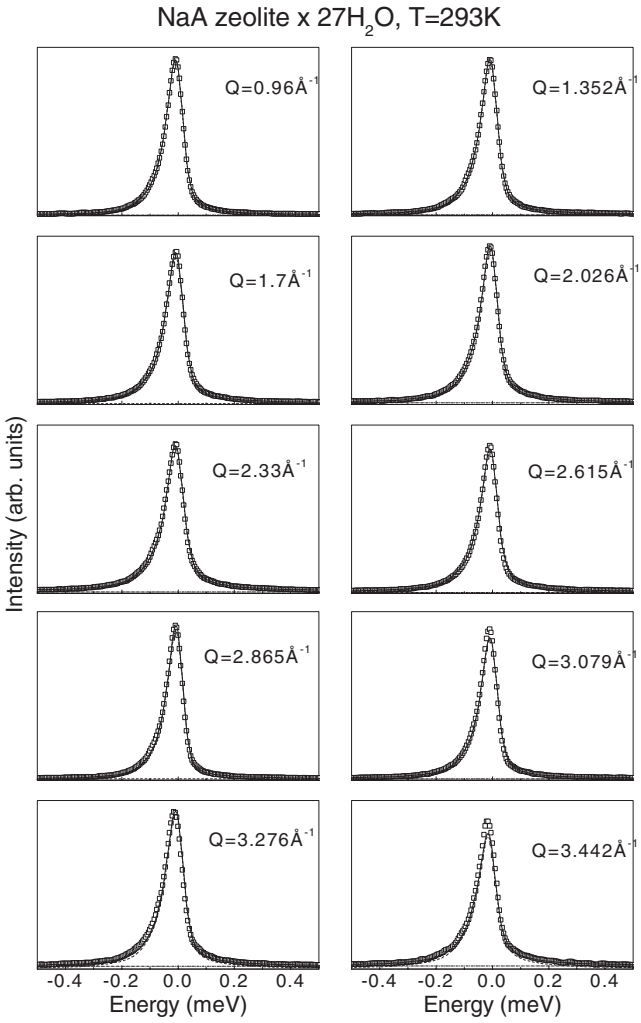

Figure 4. Experimental spectra (squares) from an IQENS experiment on NaA zeolite $\times$ $27H_2O$, at $T = 293$ K, for all the investigated Q-range, together with the best fit (solid curve) according to the RCM model and the deconvolution components (dashed curves).

In figure 4 we show the same series of high resolution IQENS data reported in figure 2, but this time reanalysed in the framework of the RCM model. As happens in the case of CDM model, the agreement is very good.

Figure 5 gives the Q-dependence of $\langle\tau\rangle$ (figure 5(A)) and β (figure 5(B)) for all the analysed temperatures. There is evidence of a power law dependence of the mean relaxation time on Q: $\langle\tau\rangle \approx Q^{-\gamma'}$. The exponent γ', extracted from the fit, turned out to be $\gamma' = -2.03$ at $T = 253$ K, $\gamma' = -2.07$ at $T = 273$ K, $\gamma' = -2.01$ at $T = 293$ K and $\gamma' = -2.07$ at $T = 313$ K. The absolute values of γ' are slightly bigger than 2. In principle, if Q is small enough, the absolute value of γ' should reduce to 2, indicating that a correct hydrodynamic behaviour is recovered.

The Q-dependence of the stretched exponent β is given in figure 5(B). In the Q-range explored, and for all the temperatures under investigation, β remains almost constant, and

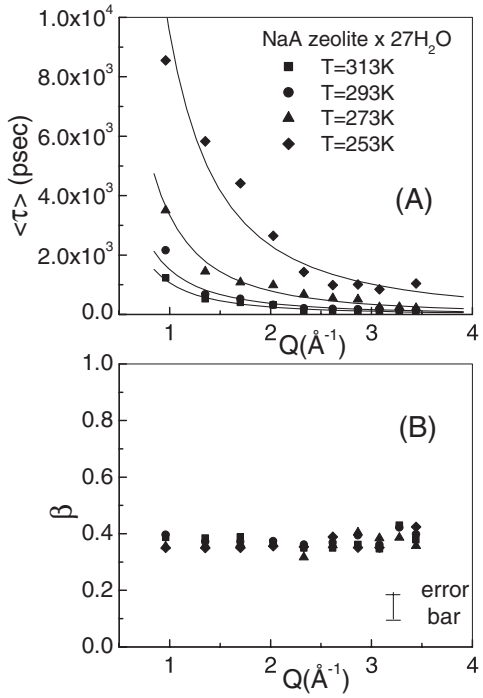

Figure 5. The Q-dependence of the mean relaxation time $\langle\tau\rangle$ (A) and of the width of the distribution β (B) for NaA zeolite $\times$ $27H_2O$ at all the analysed temperatures.

definitively less than 1. This occurrence could indicate a variety of relaxation times, i.e. a large distribution width, exhibited by the H-bonded dynamical structures even in confinement conditions. Its observed trend in temperature (β increases when T decreases) indicates a transition of liquid water from a *fragile* (high T, low β) to a *strong* (low T, high β) character [38].

Taking into account the meaningful results coming from the data analysis according to the CDM model and RCM as well, we can conclude that a choice of one interpretation with respect to the other still appears difficult.

3.2. Vibrational dynamics: FT-IR data

It is well known [39] that a typical IR spectrum is composed of a distribution of absorption vibrational bands according to the following expression:

$$A(\omega) = \sum_{\nu} (\mu^{\nu} q^{\nu})^2 \, G_{\nu}(\omega + \Omega_{\nu}) \otimes F_{1\nu}(\omega + \Omega_{\nu}) \tag{11}$$

in which q^{ν} is the νth normal coordinate, $\mu^{\nu} = (\partial\mu/\partial q^{\nu})_0$, and the terms G_{ν} and $F_{1\nu}$ represent the convoluted vibrational and rotational contributions centred at the frequencies Ω_{ν}.

In associated liquids, the highly isotropic and directional H-bond, whose energy value ranges between 2 and 6 kcal mol^{-1} and whose mean lifetime is in the picoseconds timescale, promotes a variety of intra- and intermolecular *transient* (because of the continuous breaking and reforming of the bond) arrangements [40–42]. Each of these local structures, whose degrees of association and relative population are strictly related if one takes into account the several contributions which compose the H-bond potential energy surface [43] such as

polarization, charge transfer and so on, gives rise to a different dynamic response: this justifies the appearance of peculiar bands according to the number of the possible associative species. As a consequence, the O–H stretching vibration, originally a narrow band centred at $\sim$3630 cm^{-1}, undergoes dramatic changes in frequency (red shift), shape (it spreads out over a large ω-range) and intensity, and these spectral variations can be explained on the basis of the cross-links among the inherent structures, corresponding to the various local minima in the system potential energy. This is due to the existence, for these systems, of an electrical *anharmonicity* in the dipole moment function, other than a mechanical one, that enters in the potential energy evaluation, which contributes to all nonlinear terms in the dipole moment calculations. It has been well established [44], in fact, that H-bonded systems hold an exceptional position in vibrational spectroscopy, since the first derivatives of the dipole moment $\underline{\mu}$ with respect to the coordinates of motion $\partial\underline{\mu}/\partial q_v$ are improper for the prediction of intensities I. This means that the familiar relationship

$$I = K(\partial\mu/\partial q_i)^2 \tag{12}$$

that usually expresses the intensity of an absorption band in the infrared due to the normal mode q_i, in which K is a constant that takes into account the number n_i of oscillators involved in it, is no longer valid for a strong H-bond, but can be retained true for weak H-bonded systems, as in our case.

Supposing that the time-dependent electrical field is weak (so that its interaction with the stretching mode may be treated perturbatively at the first order, and thus in a linear way with respect to the electrical field), theoretical studies of the shape of the high-frequency stretching vibration of hydrogen bonds are performed within the framework of the linear response theory [45].

According to it, the spectral density $I(\omega)$ of this stretching mode may be obtained by the Fourier transform of the autocorrelation function $G(t)$ of the dipole moment operator $\underline{\mu}$:

$$I(\omega) = \left(1/\sqrt{2\pi}\right)\int G(t)\exp\{-\mathrm{i}\omega t\}\,\mathrm{d}t \tag{13}$$

with

$$G(t) = \langle\mu^+(t)\mu(0)\rangle. \tag{14}$$

What is required to find the spectral density is the knowledge of the autocorrelation function $G(t)$ of the dipole moment operator of the fast mode averaged on some thermal properties. This autocorrelation function will differ according to the fact that the system is considered classically or quantum mechanically, and according to the hypothesis performed on the origin of the relaxation. Two main mechanisms have been considered: in the first one the fast mode, after excitation, relaxes directly toward the medium, whereas in the second, it is relaxing via the slow mode to which it is anharmonically coupled.

The O–H stretching region. Many approaches have been used to theoretically explain, in an exhaustive way, the band shapes of H-bonded systems in the O–H stretching region [46].

Some years ago, the presence of a bifurcated hydrogen bond (BHB), as one of the main features of the structure of liquid water, had been postulated for explaining the remarkable effect of temperature on the O–H stretching band observed in the Raman spectra of liquid H_2O [45]. The BHB occupies an intermediate position between the linear H-bond (LHB) and non H-bonded (NHB) OH groups. The nearest-neighbour O$\cdots$O distances are the same as in the LHB, but the apex angle is much smaller than the tetrahedral, between 95° and 100°. This allows slightly shorter second neighbour O$\cdots$O distances, and a closer packing of the

molecules. The energy of the BHB is estimated to be 2.5 kcal mol^{-1}, i.e., half that of the LHB, and its proportion in the liquid at nearly 30% at 0 °C.

Laubereau and co-workers [47, 48] interpreted the spectral substructure of the O–H stretching band of an isotopic mixture HDO in D_2O as essentially due to three contributions linked to distinct species: species I, centred at ∼3300 cm^{-1}, close to the O–H frequency for the ice structure, involving at least four strong H-bonds and small angles, giving rise an almost tetrahedral geometry; species II, peaked at ∼3400 cm^{-1}, connected to the partial formation of H bridges, generating a BHB; and species III, whose O–H frequency is centred at ∼3500 cm^{-1}, tentatively attributed to molecules involved in a weaker BHB.

Recently, Boissier and co-workers [49] decomposed the vibrational O–H stretching region of water confined in a micellar system Isooctan/AOT/H_2O into three substructures: the so-called 'connective water', at $\omega_1 \sim 3328$ cm^{-1}, corresponding to water molecules linked to three or four neighbouring H_2O molecules (species I in Laubereau's model); the 'intermediate water', at $\omega_2 \sim 3470$ cm^{-1}, representative of H_2O molecules involved in two H-bonds (species II); and the 'multimeric water', at $\omega_3 \sim 3578$ cm^{-1}, referring to molecules originating dimeric and trimeric structures.

Following the above described scenario, we were able to deconvolve our experimental IR spectra into the minimum number of symmetrical profiles. We observed three sub-bands: $\omega_1 \sim 3290$ cm^{-1}, assigned to molecules arranged in a tetrahedral 'ice-like' hydrogen bonded network; $\omega_2 \sim 3470$ cm^{-1}, assigned to water molecules arranged, by two H-bonds, in a BHB; and, finally, $\omega_3 \sim 3590$ cm^{-1}, related to H_2O molecules of monomeric structures or assembled to form dimers by linear H-bonds.

In figure 6 we report the O–H stretching (3000–3800 cm^{-1}) experimental IR spectra for NaA zeolites × $27H_2O$, at all the analysed temperatures, together with the best fit and the deconvolution components. All the parameters were left free during the fitting procedure (whose results are characterized by $r^2 \sim 0.9999$): ω_i, the sub-bands centre-frequencies, as well as the half width at half maximum (hwhm) of the used fitting profiles resulted almost T-independent; instead, a dependence on temperature was found in the case of the percentage intensities, I_i ($i = 1, 2, 3$), as shown in figure 7.

From an inspection of the figure, one immediately sees that I_1, the intensity of the ice-like ω_1 peak observed at all T, diminishes, as it should be, when T increases, from 44.6% at 278 K to 36.2% at 353 K. In contrast, I_2 increases with T, indicating that the BHB appears to be the most energetically favoured at high temperatures. I_3 seems not to be influenced by T, at least in the T-range explored, and, with it, the relative population of monomers or dimeric structures triggered by LHB.

We also collected, at room temperature ($T = 293$ K), IR data varying the hydration percentage, and in particular for NaA zeolite × $27H_2O$ (fully hydrated sample) and NaA zeolite × $6H_2O$ (partially hydrated sample). In figure 8 we show the corresponding experimental IR spectra together with the theoretical best fit and the deconvolution components. For comparison, the IR spectrum of bulk water at $T = 293$ K is also shown. The filled area refers to the tetrahedral ice-like sub-band, dominant in the bulk state, that, as appears clear, is still present under confinement at the full and low hydration regime.

These experimental results allow us to hypothesize a 'structure-maker' role of zeolitic surface on confined water, since the strong clustering of water molecules cannot be easily broken up by the thermal motion, nor by the surface interactions.

Finally, we want to show here the preliminary result obtained very recently from an analysis, actually in progress, performed to investigate, always as a function of temperature and for different amount of adsorbed water molecules, the dynamics of water entrapped in Mg-exchanged A-type zeolites. With the exchange of Na ions with Mg ions, having then modified

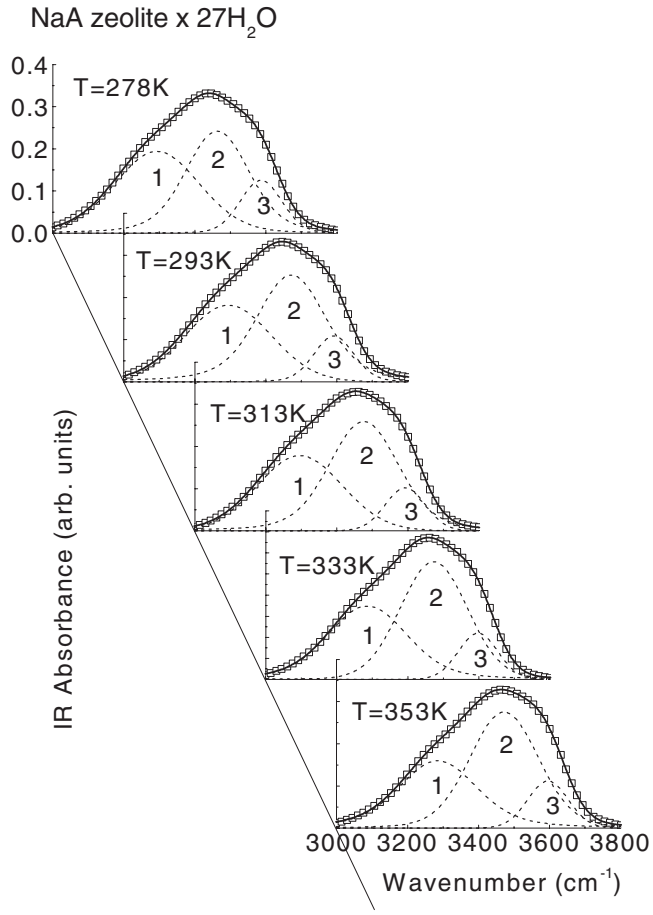

Figure 6. The experimental IR O–H stretching band (squares) of NaA zeolite $\times$ $27H_2O$ plotted, as a function of T, together with the best fit (continuous curve) and the deconvolution components (dashed curves).

the zeolitic matrix in the active part in the interaction with water, it is possible to perform an energetic separation of the water state in the void, as revealed by differential thermo-gravimetric experiments performed by Mizota. A strong variation in the water dynamics is then expected, since the ionic strength of the added Mg, being different from that of Na, induces different ion–dipole interaction.

In figure 9 we report the experimental O–H stretching IR band of Mg(50)Na(50)A zeolite $\times$ $27H_2O$, together with the best fit and the deconvolution sub-bands. This sample differs from the NaA zeolite investigated here, since 50% of the Na ions have been substituted with Mg ions. The spectrum has been fitted and interpreted, as in the case of NaA zeolites, always in the framework of the model suggested by Boissier and co-workers [49].

The 'connective' (at $\sim$3290 cm^{-1}), 'intermediate' (at $\sim$3470 cm^{-1}) and 'multimeric' (at $\sim$3590 cm^{-1}) contributions have also been revealed in this case. But, as appears immediately clear from an inspection of figure 9, the ice-like sub-band has the highest percentage intensity ($I_1 \sim 72.5\%$). This occurrence indicates that the tetrahedral network typical of bulk water remains the one favoured even under confinement, suggesting that the partial exchange of Na with Mg ions enhances the 'structure-maker' role of zeolitic surface.

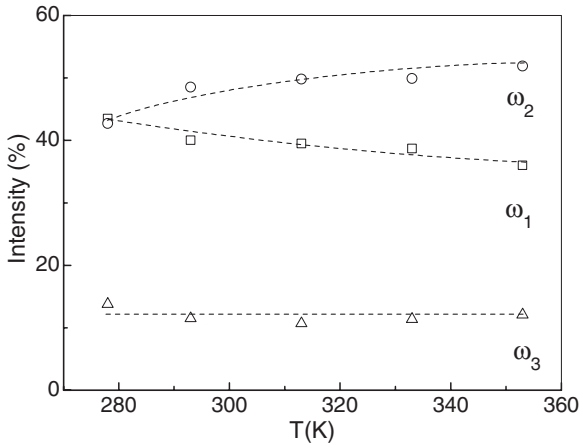

Figure 7. The T-dependence of the percentage intensities in the case of NaA zeolite $\times$ $27H_2O$, of the different sub-bands, as extracted from the best fit procedures. The dashed lines are guides for the eyes.

We want to remark, now, that an exactly opposite trend was observed in the case of water confined in a sol–gel silica glass, GelSil, of 25 Å diameter pores, whose structural and dynamical properties have been the focus of our attention in recent years [11, 12, 30]. We recall here the main results obtained by our group as far as the vibrational properties are concerned, for a meaningful comparison with zeolitic water.

In figure 10(A) we show, as an example, the one-phonon proton effective vibrational density of states (VDOS), $Z(\omega)$, for confined water at $T = 20\,^{\circ}\mathrm{C}$ and hydration percentages $N/N_0 = 100\%$ and 5%, together with the best fit and the deconvolution Gaussian components. The data have been obtained by incoherent inelastic neutron scattering (IINS) measurements performed by means of the IN6 t.o.f. spectrometer at ILL, Grenoble, France, as a function of temperature and at different hydration levels [11]. Also in this case, the VDOS for bulk water at the same temperature is shown for comparison. The lowest-frequency sub-bands, centred at $\sim$8 and $\sim$20 meV, are identifiable as the bending and O $\cdots$ O stretching intermolecular modes of water. Moving to higher frequencies, we observed three sub-bands, centred at $\sim$52, 70 and 91 meV respectively, connected to the librational modes around the three symmetry axis of water molecule.

As can be seen, the IINS spectra of water in GelSil, generally dominated by the librational contribution, revealed, with respect to bulk water, (i) a flattening and attenuation of the hindered translational modes (8 and 20 meV), indicating a strong destructuring effect in the interfacial water, and (ii) an enhancement of the librational modes at $\sim$91 meV, mainly connected with the hindered rotation of water bonded with two silanol (Si–OH) groups present on the inner surface of the matrix [50]. This allowed us to attribute a 'structure-breaker' role of GelSil, since under confinement, and in particular diminishing the hydration percentage, the symmetries typical of the bulk state are lost because of the specific interaction (H-bond) among the interfacial H_2O and the surface Si–OH groups. These IINS data are, however, in full agreement with our previous Rayleigh-wing measurements performed always on water in 25 Å pores of GelSil [12]. In that case, in order to explain the restricted translational region spectra, we adopted a solid state point of view, and we reduced the data for obtaining the effective susceptibility $\chi''(\omega)$ (*à la mode MCT*) by the relation

$$\chi''(\omega) = I_{\mathrm{VH}}(\omega)\,(n(\omega, T) + 1)^{-1} \tag{15}$$

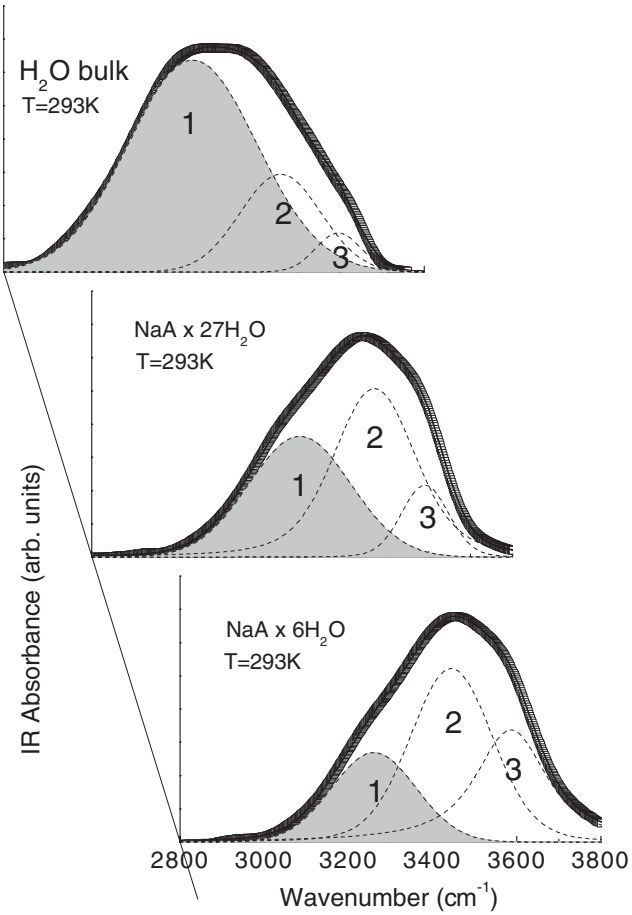

Figure 8. The experimental IR O–H stretching band (squares) of H_2O bulk, NaA zeolite $\times$ $27H_2O$, NaA zeolite $\times$ $6H_2O$, plotted, at $T = 293$ K, together with the best fit (continuous curve) and the deconvolution components (dashed curves).

where $I_{\mathrm{VH}}(\omega)$ is the depolarised Rayleigh wing intensity, and $n(\omega, T) + 1$ is the well-known Bose–Einstein population factor. From $\chi''(\omega)$ we extracted the effective Raman vibrational density of states:

$$g^{\mathrm{R}}_{\mathrm{eff}}(\omega) = \omega\chi''(\omega) = \sum_b P_b(\omega) g_b(\omega) \tag{16}$$

where $P_b(\omega)$ is the electron-vibrational coupling function, $g_b(\omega)$ the *true* amplitude weighted VDOS (obtained in an IINS experiment), and the summation is extended to the various bands b.

Figure 10(B) reports, for comparison with IINS spectra, the Raman effective VDOS for water in the bulk state and confined in GelSil at $N/N_0 = 100\%$ and $N/N_0 = 5.9\%$, always at $T = 20\,^{\circ}\mathrm{C}$. In the case of bulk water, $g^{\mathrm{R}}_{\mathrm{eff}}(\omega)$ is induced by localized vibrational excitations of the molecules, and reveals the two characteristic large bumps identified as HB bending (the lowest one, convoluted with the acoustical like contribution) and HB stretching lattice vibrations. As can be seen, the lowering of the water content inside the glass causes a flattening of $g^{\mathrm{R}}_{\mathrm{eff}}(\omega)$ spectral profile, indicating the disappearance, under confinement, of the two collective modes dominant in the bulk.

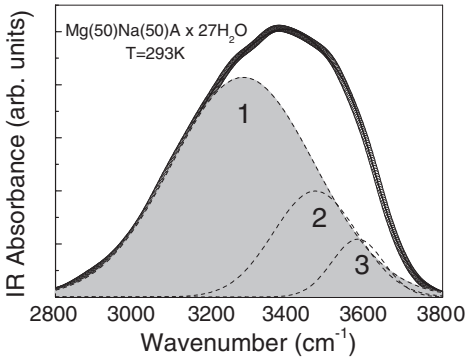

Figure 9. The experimental IR O–H stretching band (circles) of Mg(50)Na(50)A zeolite × $27H_2O$, plotted, at $T = 293$ K, together with the best fit (continuous curve) and the deconvolution components (dashed curves).

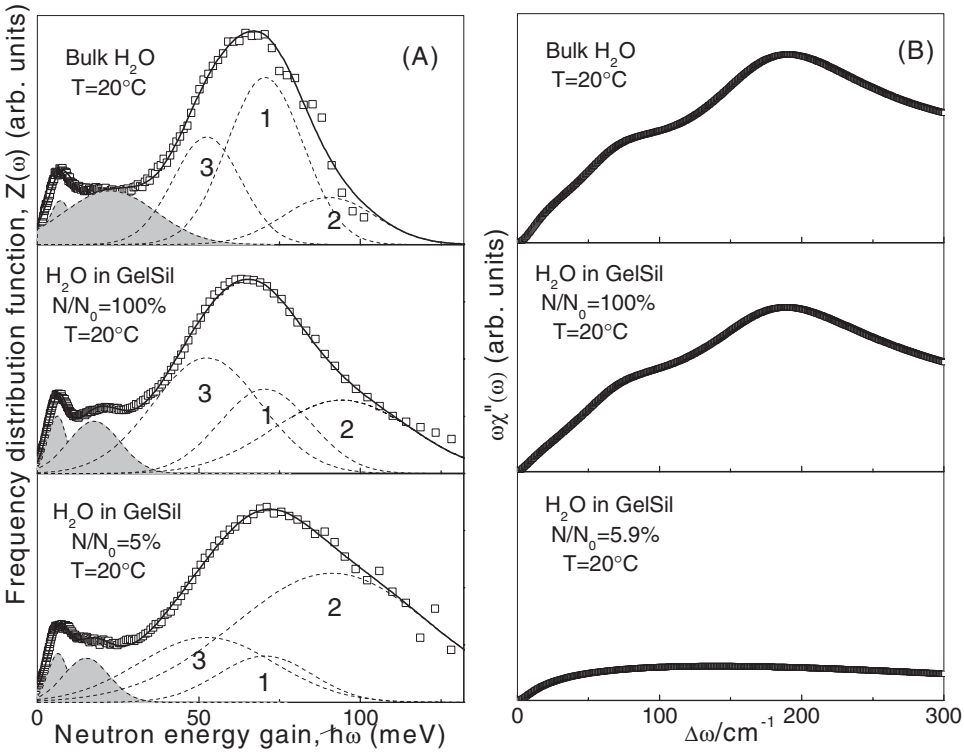

Figure 10. The one-phonon proton effective VDOS as obtained from IINS experiments ((A), squares), and Raman effective VDOS as obtained from Rayleigh wing measurements ((B), squares), for H_2O bulk and confined in GelSil 25 Å, in full and partial hydration conditions.

The H_2O bending region. We also studied the effects of confinement by an analysis of the evolution of the H_2O bending band, as a function of hydration level, from bulk H_2O, for which, as is well known, it has a maximum centred at $\sim$1640 cm^{-1}, to NaA × $27H_2O$ and NaA × $6H_2O$.

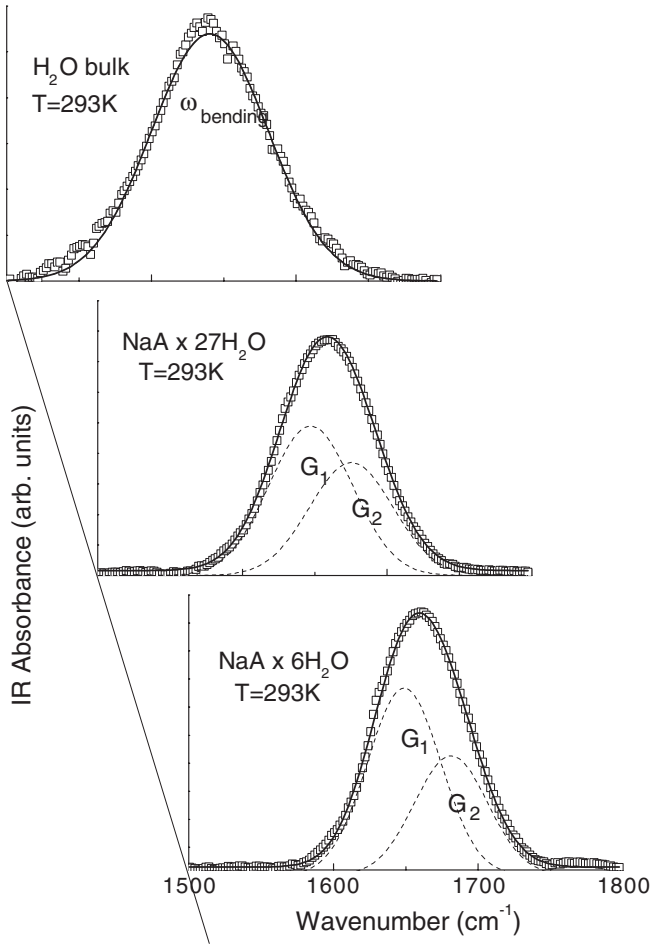

Figure 11. The experimental IR H_2O bending band (squares) of H_2O bulk, NaA zeolite $\times$ $27H_2O$, NaA zeolite $\times$ $6H_2O$, plotted, at $T = 293$ K, together with the best fit (continuous curve) and the deconvolution components (dashed curves).

We deconvolved the H_2O bending band into the minimum number of Gaussian profiles, leaving all the parameters free during the fitting procedure.

The corresponding experimental IR spectra, together with the best fit and the deconvolution components, are shown in figure 11.

For confined water we observed two components, G_1 and G_2, centred, respectively, at $\sim$1648 and $\sim$1678 cm^{-1}. As far as the percentage intensities I_{G1} and I_{G2} are concerned, we observed that, with the diminishing of the water content, I_{G1} increases from 47.4% to 50.3%, whereas I_{G2} decreases from 35.8% to 32.1%. Their trend recalls the one observed for 'connective' and 'intermediate' water, i.e. ω_1 and ω_2 sub-bands in the O–H stretching spectra, the first one decreasing passing from the highest to the lowest water content, the second one increasing. On the basis of this analogy, we related the lower energy H_2O bending Gaussian component, G_1, to the 'intermediate' H_2O molecules, and the higher energy component, G_2, to the 'connective' ice-like H_2O.

A deeper analysis of this mode, as a function of temperature, is in progress.

4. Conclusions

In this review paper we have presented a few of our most meaningful results, obtained from detailed incoherent quasi-elastic neutron scattering (IQENS) and Fourier transform infrared absorption (FT-IR), on the diffusive and vibrational properties of water molecules encaged in nanopores of hydrated NaA zeolite, as a function of temperature and hydration level.

As far as the diffusive properties are concerned, the IQENS data analysis has been performed in the light of a confined diffusion model (CDM) and a relaxing cage model (RCM). The main results can be summarized in the following way.

(i) In the framework of the CDM model, based on the Volino–Dianoux model for confined diffusion in a potential of spherical symmetry, we observed a Q-dependence of the half width at half maximum (hwhm, Γ) of the Lorentzian quasi-elastic peak: a constant value is assumed at low Q as a consequence of confinement, and it is maintained until a Q^* value whose inverse gives an idea of the size of the confining region. In our case, $Q^* = 2.02\ \text{Å}^{-1}$ and, from it, $l^* = 3.11$ Å, for all the analysed temperatures. Then, a random jump diffusion behaviour is recovered. It starts at very high Q, indicating that we are in the presence of a *local* diffusion process recalling the 'flip-flop' H-bond process of the proton tunnelling observed in ice.

(ii) According to the RCM model, which considers the IQENS spectra as a single quasi-elastic peak reflecting a distribution of relaxation times, described by an Havriliak–Negami profile, we observed a Q-dependence of the mean relaxation time $\langle\tau\rangle$ and of the width β of the distribution. In particular, as far as the mean relaxation time is concerned, a power law dependence, $\langle\tau\rangle \sim Q^{-\gamma'}$, has been found in the Q-range explored, with an exponent γ' that turned out to be $\widetilde{=} -2$ at all the analysed temperatures, revealing an almost continuous diffusion. The behaviour, as a function of Q, of β could suggest a fragile (high T, low Q)–strong (low T, high Q) behaviour transition for liquid water.

This hierarchy of different structural arrangements, at the basis of the observed distribution of relaxation times, is in full agreement with the presence of different species. These last were observed from the analysis of the vibrational properties of confined water, performed, by means of FT-IR absorption, in the O–H stretching (3000–3800 cm^{-1}) and in the H_2O bending (1500–1800 cm^{-1}) spectral regions. In particular, the existence of a bifurcated hydrogen bond (BHB) between three molecules has been postulated as a main feature of the structure of liquid water in bulk and in the confined state. Nevertheless, the most interesting result regards the presence, at all the analysed temperatures, of the contribution linked to the tetrahedral ice-like substructures, whether in the fully hydrated zeolite ($27H_2O$ molecules) or in the partially hydrated ($6H_2O$ molecules) one, definitely in contrast with the trend revealed by our previous incoherent inelastic neutron scattering (IINS) and Rayleigh wing measurements performed, at the same temperature conditions and at the same hydration level, on water confined into a glassy matrix, GelSil, with hydrophilic inner surface. A comparison among the data from all these different and complementary spectroscopic techniques allowed us to suggest the 'structure-maker' role of the zeolitic surface on the vibrational dynamics of water, as opposed to the 'structure-breaker' character of GelSil glass.

The deconvolution of the H_2O bending mode revealed two Gaussian sub-bands that behave, when the hydration level decreases, like the spectral substructures revealed for the O–H stretching vibration.

Actually, a further investigation of the connectivity properties of water in restricted geometry is in progress, using Mg-exchanged A-type zeolites as the confining medium. From

a preliminary IR analysis, in fact, the 'structure-maker' role of zeolites seems to be enhanced by the partial exchange, on the inner surface of the pores, of Na ions with Mg ions.

References

[1] Chen S H 1991 *Hydrogen-Bonded Liquids* (*NATO Advanced Study Institute Series C: Mathematical and Physical Sciences* vol 329) ed J C Dore and J Teixeira (Dordrecht: Kluwer) p 289
[2] Ricci M A, Bruni F, Gallo P, Rovere M and Soper A K 2000 *J. Phys.: Condens. Matter* **12** A345
[3] Dore J C, Coveney F and Bellissent-Funel M C 1992 *Recent Developments in the Physics of Fluids* ed W S Howells and K Soper (Bristol: Hilger) p 299
[4] Venuti V, Crupi V, Magazù S, Majolino D, Migliardo P and Bellissent-Funel M C 2000 *J. Physique* IV **10** 7-211
[5] Careri G 1998 *Prog. Biophys. Mol. Biol.* **70** 233
[6] Bruni F, Ricci M A and Soper A K 1998 *J. Chem. Phys.* **109** 1478
[7] Soper A K, Bruni F and Ricci M A 1998 *J. Chem. Phys.* **109** 1486
[8] Bellissent-Funel M C, Chen S H and Zanotti J M 1995 *Phys. Rev.* E **51** 4558
[9] Zanotti J M, Bellissent-Funel M C and Chen S H 1999 *Phys. Rev.* E **59** 3084
[10] Soper A K 1991 *Hydrogen-Bonded Liquids* (*NATO Advanced Study Institute Series C: Mathematical and Physical Sciences* vol 329) ed J C Dore and J Teixeira (Dordrecht: Kluwer) p 147
[11] Crupi V, Majolino D, Migliardo P and Venuti V 2002 *J. Phys. Chem.* B **106** 10884
[12] Crupi V, Magazù S, Majolino D, Maisano G and Migliardo P 1999 *J. Mol. Liq.* **80** 133
[13] Fouzri A, Dorbez-Sridi R and Oumezzine M 2002 *J. Chem. Phys.* **116** 791
[14] Polnazek C F and Bryant R G 1984 *J. Chem. Phys.* **81** 4038
[15] Barthel J, Bachhuber K, Buchner R and Hetzenauer H 1990 *Chem. Phys. Lett.* **165** 369
[16] Lynden-Bell R M and Rasaiah J C 1996 *J. Chem. Phys.* **105** 9266
[17] Zhu S B and Robinson G W 1991 *J. Chem. Phys.* **94** 1403
[18] Gallo P, Rovere M and Sphor E 2000 *Phys. Rev. Lett.* **85** 4317
[19] Huwe A, Kremer F, Beherns P and Schwieger W J 1999 *Phys. Rev. Lett.* **82** 2338
[20] Gallo P, Rovere M, Ricci M A, Harting C and Sphor E 1999 *Phil. Mag.* B **79** 1923
[21] Gallo P 2000 *Phys. Chem. Chem. Phys.* **2** 1607
[22] Crupi V, Dianoux A J, Majolino D, Migliardo P and Venuti V 2002 *Phys. Chem. Chem. Phys.* **6** 2768
[23] Crupi V, Majolino D, Migliardo P, Venuti V and Dianoux A J 2002 *Appl. Phys.* A **74** S555
[24] Mizota T, Satake N, Fujiwara K and Nakayama N 2000 Steam, water and hydrothermal systems: physics and chemistry meeting the needs of industry *Proc. 13th ICPWS* ed P R Tremaine, P G Hill, D E Irish and P V Balakrishnan (Ottawa: NCR Research Press)
[25] Johnson G K, Flotow H E, O'Hare P A G and Wise W S 1982 *Am. Mineral.* **67** 736
[26] Volino F and Dianoux A J 1980 *Mol. Phys.* **41** 271
[27] Chen S H, Liao C, Sciortino F, Gallo P and Tartaglia P 1999 *Phys. Rev.* E **59** 6708
[28] Crupi V, Magazù S, Maisano G, Majolino D, Migliardo P and Venuto S 1994 *Phys. Chem. Liq.* **26** 263
[29] Gramlich V and Meier W M 1971 *Z. Kristallogr.* **133** 134
[30] Crupi V, Majolino D, Migliardo P and Venuti V 2000 *J. Phys. Chem.* A **104** 11000
[31] Bellissent-Funel M C, Zanotti J M and Chen S H 1996 *Faraday Discuss.* **103** 281 and references therein
[32] Bellissent-Funel M C 2002 *J. Mol. Liq.* **96/97** 287
[33] Gotze W and Sjogren L 1992 *Rep. Prog. Phys.* **55** 241
[34] Dianoux A J, Pineri M and Volino F 1982 *Mol. Phys.* **46** 129
[35] Wanderlingh U N, Giordano R, Dianoux A J and Wanderlingh F 2002 *Physica* A **304** 276
[36] Alvarez F, Alegria A, Colmenero J, Alberdi J M and Frick B 1991 *Phys. Rev.* B **44** 7321
[37] Alvarez F, Alegria A and Colmenero J 1991 *Phys. Rev.* B **44** 7306
[38] Ito K, Moyniham C T and Angell C A 1999 *Nature* **389** 492
[39] Clark R J H 1978 *Advances in Infrared and Raman Spectroscopy* ed R J H Clark and R E Hester (London: Heyden) p 109
[40] Crupi V, Jannelli M P, Magazù S, Maisano G, Majolino D and Migliardo P 1994 *Phys. Chem. Liq.* **28** 117
[41] Crupi V, Maisano G, Majolino D, Migliardo P and Musolino A M 1998 *Nuovo Cimento* D **20** 2191
[42] Crupi V, Maisano G, Majolino D, Migliardo P and Venuti V 2000 *J. Phys. Chem.* A **104** 3933
[43] Kollman P A and Allen L C 1972 *Chem. Rev.* **72** 283
[44] Janoschek R 1976 *The Hydrogen Bond* vol 1, ed P Shuster, G Zundel and C Sandorfy (Amsterdam: North-Holland) p 166
[45] Henri-Rousseau O and Blaise P 1997 *Theoretical Treatments of Hydrogen Bonding* ed D Hadzi (New York: Wiley) p 165

[46] Giguere P A 1984 *J. Raman Spectrosc.* **15** 354
[47] Laenen R, Rauscher C and Laubereau A 1998 *J. Phys. Chem.* B **102** 9304
[48] Graener H, Seifert G and Laubereau A 1991 *Phys. Rev. Lett.* **66** 2092
[49] Boissier C, Brubach J B, Mermet A, De Marzi G, Bourgaux C, Prouzet E and Roy P 2002 *J. Phys. Chem.* B **106** 1032
[50] Steytler D C, Dore J C and Wright C J 1983 *Mol. Phys.* **48** 1031